scientific reports

Check for updates

OPEN

Baseline neuroimaging profiles and predictive modelling for early Alzheimer disease prognosis

Aleix Martí-Navia[1,4], Alejandro López-Bellido[1,4], Ángel Balaguer[2], Sara Ballesta-Martínez[1], Lourdes Álvarez-Sánchez[1,3], Mar Peretó[1], Lorena García-Vallés[1], Luis Raga[1], Miguel Baquero[1,3] & Consuelo Cháfer-Pericás[1]✉

Alzheimer's disease (AD) presents significant clinical heterogeneity in cognitive decline. Neuroimaging profiles and peripheral biomarkers, such as plasma oxidative stress biomarkers could provide information on AD progression. This study evaluates the contribution of baseline neuroimaging features and plasma lipid peroxidation biomarkers to modelling cognitive decline trajectories in early AD. Data were collected from patients with early AD (n = 195), and they were neuropsychologically evaluated to assess their progression. Baseline data included demographics, neuropsychological evaluations, neuroimaging measures and plasma lipid peroxidation levels. Follow-up neuropsychological evaluations were conducted biennially. Individual cognitive decline trajectories were estimated using MMSE and CDR Sum of Boxes (CDR-SB) scores. Multivariate modelling and hierarchical clustering analyses were applied to identify prognostic signatures and patient subgroups. Baseline neuroimaging variables showed significant associations with longitudinal cognitive trajectories, as reflected in MMSE and CDR Sum of Boxes slopes, whereas plasma lipid peroxidation biomarkers did not. Multivariate models based on neuroimaging features demonstrated substantial predictive contribution (conditional R^2 0.825 for MMSE and 0.808 for CDR Sum of Boxes). Hierarchical clustering identified four distinct groups, primarily driven by left Koedam scores, enlarged perivascular spaces, and Fazekas scores. These clusters were significantly associated with differential rates of cognitive decline, particularly for MMSE. In conclusion, structural neuroimaging measures at baseline are robust indicators of cognitive decline in early AD, supporting its utility for individualized prognosis in early AD.

Keywords Alzheimer disease, Lipid peroxidation, Neuroimaging, Prognosis

Alzheimer's disease (AD), the predominant cause of dementia worldwide, is characterized by progressive cognitive decline[1]. The neuropathological hallmarks of AD encompass extracellular deposition of amyloid-beta (Aβ) peptides forming senile plaques, intracellular aggregation of phosphorylated tau protein constituting neurofibrillary tangles, and reactive astrogliosis marked by elevated expression of molecules like glial fibrillary acidic protein (GFAP) in regions adjacent to Aβ plaque[2]. Current AD diagnosis relies predominantly on the quantification of pathological biomarkers in cerebrospinal fluid (CSF) samples[3] or visualization of amyloid deposition via positron emission tomography (PET) imaging[4], providing the information for AT classification[5]. Nevertheless, AD evolution in initial stages shows a significant clinical heterogeneity, with substantial inter-individual variability in disease progression and phenotypic presentation[6]. However, few studies evaluating AD progression heterogeneity from baseline variables are available in the literature.

The progression of early AD stages to dementia has become a focal point for researchers seeking to identify predictive biomarkers and risk factors[7–9]. However, a few recent prognosis studies are based on cognitive decline rate, measured by Mini-Mental State Examination (MMSE) or Rey Auditory Verbal Learning Test (RAVLT)[10], as well as Clinical Dementia Rating-sum of boxes (CDR-SB)[11], and Repeatable Battery of the Assessment of Neuropsychological Status (RBANS) delayed memory[12,13], which is crucial to bring more information about disease progression.

[1]Alzheimer's Disease Research Group, Instituto de Investigación Sanitaria La Fe, Avda de Fernando Abril Martorell, 106, 46026 Valencia, Spain. [2]Plataforma de Big Data, IA y Bioestadística, Instituto de Investigación Sanitaria La Fe, 46026 Valencia, Spain. [3]Division of Neurology, Hospital Universitari I Politècnic La Fe, 46026 Valencia, Spain. [4]These authors contributed equally to this work: Aleix Martí-Navia and Alejandro López. ✉email: m.consuelo.chafer@uv.es; consuelo_chafer@iislafe.es

Regarding prognosis predictors, some plasma biomarkers (neurofilament light polypeptide (NfL), brain-derived tau (BD-tau), phosphorylated tau 217 (p-Tau217), p-Tau 181, GFAP, and Aβ42/Aβ40) have been used to study the AD prognosis[14,15]. These studies showed that plasma biomarkers can be used for the prediction of clinical decline, clinical progression, and associations with dementia stage progression. Moreover, a recent study incorporated demographic data and routine laboratory parameters to plasma p-Tau217, as prognosis variables[16], developing a predictive model to monitor AD progression before the onset of cognitive symptoms. In addition, some biomarkers of protein oxidation were studied for AD prognosis[17]. However, despite the effects of oxidative stress and reactive oxygen/nitrogen species on neuroinflammation[18], few studies have evaluated their relationship with AD progression[19,20]. In addition, neuroimaging (MRI) may represent a useful approach for studying the progression and cognitive decline trajectories of AD patients[21,22]. In fact, a recent study based on MRI focused on the detection of fast cognitive decline and the risk of progression to mild cognitive dementia (MCI)[23]. Also, a predictive model based on structural T1-weighted MRI, [^{18}F]-fluorodeoxyglucose-PET, amyloid PET, neuropsychological assessments, and demographic variables was developed to predict cognitive decline in AD[24].

When it comes to AD physiopathology, recent studies indicate that AD comprises multiple subtypes, prompting various research groups to investigate how co-pathologies relate to these different forms of the disease[25]. These subtypes generally align with classifications based on neuropathological features, MRI patterns, and clinical presentation[26]. Neuropathological and MRI-based analyses have identified four major AD subtypes: typical, limbic-predominant, hippocampal-sparing, and minimal atrophy[26]. Additionally, clinical phenotypes have revealed further variants of AD, including the amnestic, logopenic primary progressive aphasia, behavioral, and corticobasal syndrome presentations[27,28]. Therefore, research using multimodal biomarkers (clinical, biochemical etc.) remains crucial[13,29,30]. Combining MRI with blood-based biomarkers has shown promise for identifying individuals at increased risk of AD[31] and for predicting subsequent cognitive decline[32]. The integration of molecular biomarkers, structural brain imaging, and neuropsychological evaluations holds significant potential to improve prognostic accuracy in the early stages of AD[33–35].

This study aims to evaluate the multimodal contribution of baseline MRI measures and plasma lipid peroxidation biomarkers levels to modelling cognitive decline trajectories in patients with AD at early stages.

Methods

Study design and participant selection

A longitudinal observational study (2018-present) was conducted at the Cognitive Impairment Unit of Hospital Universitari i Politècnic La Fe (Valencia, Spain) to evaluate prognosis in AD. Participants included patients diagnosed with early AD (presymptomatic, mild cognitive impairment (MCI), or mild dementia) based on CSF biomarkers and neuropsychological tests.

Inclusion criteria were age between 50 and 80 years old, CSF Aβ42/Aβ40 < 0.069[36] or positive amyloid PET, but no impairment or only minor impairment in carrying out activities of daily living, in accordance with NIA-AA criteria[37]. The CSF biomarkers were measured using chemiluminescence immunoassay (CLIA) (Lumipulse® G, Fujirebio, Tokyo, Japan).

Exclusion criteria included the presence of other neurological disorders (e.g., traumatic brain injury, epilepsy, brain damage, stroke, multiple sclerosis…) that could cause cognitive impairment, severe psychiatric disorders (major depression, bipolar disorder, schizophrenia…), severe dementia, or any condition that prevented adequate neurological assessment.

At the time of diagnosis (T1, baseline), demographic (age, sex, educational level), molecular (plasma biomarkers, ApoE genotype), neuroimaging (MRI) and neuropsychological data were collected from participants (n = 226). Approximately every two years (T2, T3, T4, T5), these patients were neuropsychologically evaluated to assess their progression (n = 195).

This study was conducted in accordance with the Declaration of Helsinki, and it was approved by the Ethics Committee from Instituto de Investigación Sanitaria La Fe (Valencia, Spain) (Reference number: 2022–282-1, Date: 29/03/2023, and 2022–990-1, date: 08/02/2023). All participants signed informed consent before their recruitment.

Neuropsychological evaluation

Certified neuropsychologists conducted the neuropsychological assessment. It included the CDR with six domains (memory (CDR-M), orientation (CDR-O), judgment and problem solving (CDR-JPS), community affairs (CDR-CA), home and hobbies (CDR-HH), personal care (CDR-PC)), a global CDR score (CDR-GS) and CDR-SB[38,39], MMSE[40,41], RBANS with five domains (immediate memory (RBANS-IM), visuospatial/constructional (RBANS-V/C), language (RBANS-L), attention (RBANS-A), delayed memory (RBANS-DM))[42–44], Functional Activities Questionnaire (FAQ)[45], Alzheimer's Disease Cooperative Study – Activities of Daily Living (ADCS-ADL)[46] and Geriatric Depression Scaled (GDS)[26]. The cut-off values used to identify MCI-AD patients at T1 were CDR-GS ≤ 0.5, MMSE score between 23 and 27, and RBANS-DM < 85, with at least two of these criteria required.

After diagnosis (T1), participants underwent neuropsychological evaluation (MMSE, CDR) approximately every two years to identify different trajectories of cognitive decline. Figure 1 shows the follow-up scheme of these patients. Some patients were unable to complete follow-up visits T2–T5 for several reasons (death, refusal to continue participation, or inability to attend the neuropsychological evaluation). Specifically, patients with only one available time point were excluded from the present study. The reasons for their exclusion were withdrawal (51%), death (23%), severe deterioration with institutionalization (14.3%), inability to be contacted (5.7%) and unknown reasons (5.7%).

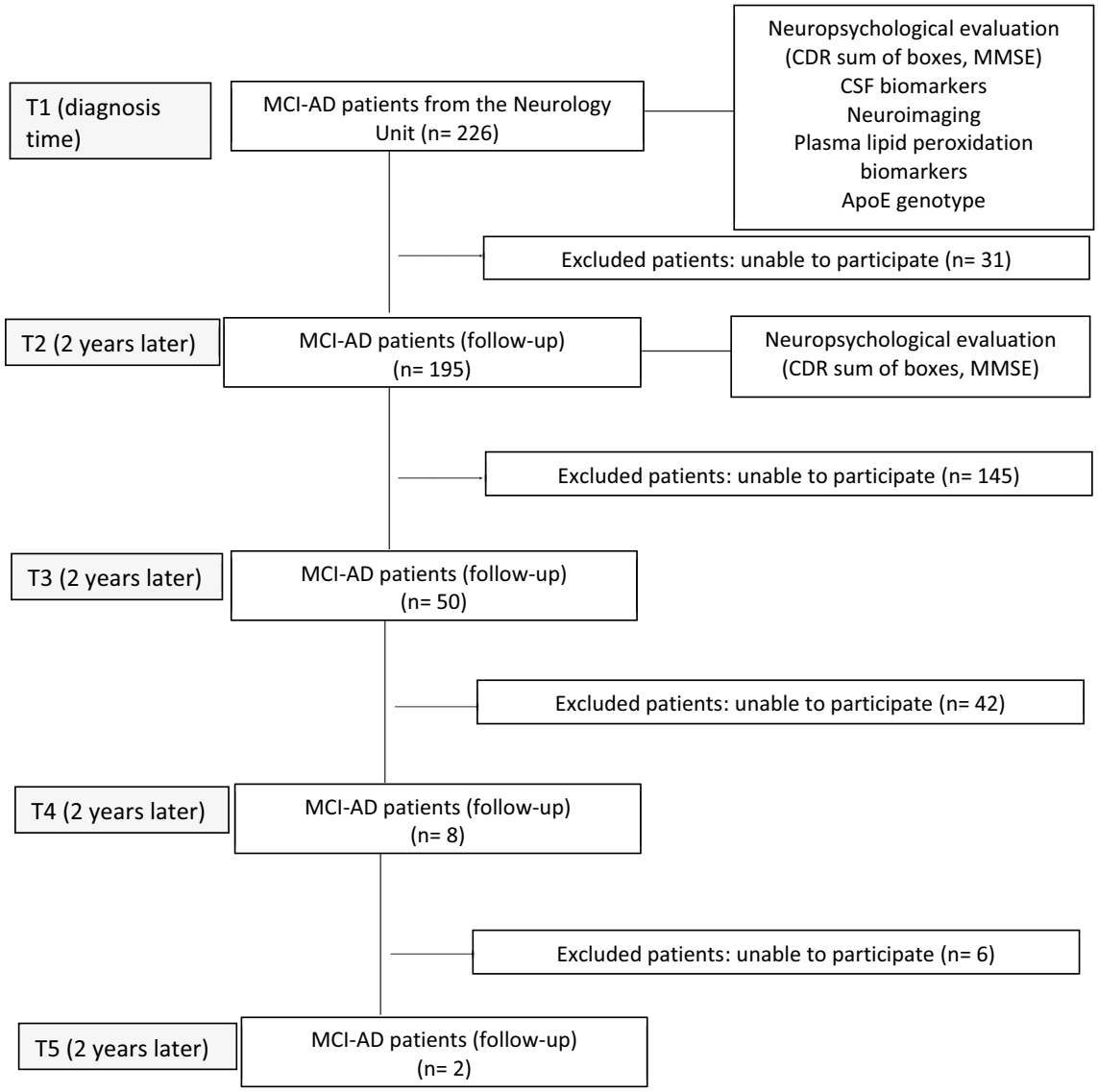

Fig. 1. Study flow diagram. The selection and longitudinal follow-up process of patients with AD-type mild cognitive impairment (MCI-AD) is shown, from the time of diagnosis (T1) to eight years later (T5), with biennial assessments.

Clinical progression of AD patients

The longitudinal progression of CDR Sum of Boxes and MMSE scores was obtained from the dates and the scores obtained at each neuropsychological evaluation (T1-T5). For each participant, the time elapsed in years from T1 to subsequent assessments (T2–T5) was calculated, providing a continuous measure of follow-up duration.

Plasma samples treatment and analysis

Blood samples were obtained at baseline (T1) via venous puncture into EDTA-containing tubes. The samples were centrifuged at room temperature for 15 min at 1160 g, and the plasma fraction was transferred to a new tube containing butylated 8-hydroxytoluene (BHT) (0.25% (w/v) in ethanol) to prevent further oxidation of the sample. The plasma samples were stored at −80 °C until analysis.

For lipid peroxidation compounds determination, sample treatment was previously described by Peña-Bautista et al.[47]. Briefly, 5 µl of an internal standard solution ($PGF_{2\alpha}$-D4 2 µmol L^{-1} and D4-10-epi-10-F_{4t}-NeroP 1.2 µmol L^{-1}) and 400 µL of a potassium hydroxide solution (15% w/v) were added to 400 µL of plasma to carry out the hydrolysis (40 ºC, 30 min). Then, proteins were precipitated with HCl, and the supernatant pH was 3–4. After that, samples were purified by solid phase extraction in order to preconcentrate analytes and minimize interferences. Finally, the extract was evaporated and reconstituted to be analysed by ultra-performance liquid chromatography coupled to tandem mass spectrometry (UPLC-MS/MS), as described in a previous study[48]. The lipid peroxidation compounds (15(*R*)−15-F_{2t}-IsoP, PGE2, 2,3-dinor-iPF2 αIII, 15-keto-15-E_{2t}-IsoP, 15-keto-

15-F_{2t}-IsoP, 15-E_{2t}-IsoP, 15-F_{2t}-IsoP, 5-F_{2t}-IsoP, $PGF_{2\alpha}$, 1a,1b-dihomo-$PGF_{2\alpha}$) were purchased from Cayman Chemical Company (Ann Arbor, Michigan, USA)[48].

Neuroimaging visual analysis

MRI scans (t1, FLAIR, t2, t2*) at baseline were analyzed using different standardized scales. The corresponding results were measures of medial temporal atrophy (Scheltens score)[49], posterior parietal atrophy (Koedam score)[50], degree of white-matter lesions secondary to microangiopathy (Fazekas score)[51], quantitative analysis of microbleeds, and dilated perivascular spaces in the basal ganglia, cortical regions, midbrain, and/or temporo-insular areas. Atrophy was evaluated using T1 sequence with repetition time (RT) 5.7 ms, echo time (ET) 2.1 ms, and slice thickness (ST) 1.2 mm; white-matter lesions and perivascular spaces were analyzed with T2/FLAIR (ST 5 mm); and microbleeds were evaluated in T2* sequences (ST 5 mm). All neuroimaging visual analysis were performed by a single observer so there is no inter-rater variability.

Statistical analysis

The association between all the biomarkers (lipid peroxidation compounds, MRI features) and longitudinal cognitive performance was evaluated using the MMSE and CDR-SB scores as outcome measures; and the date for the first neuropsychological assessment (T1) was used as temporal reference. For each biomarker, a univariate linear mixed-effects model was fitted, including random intercepts and slopes for each subject, but without estimating their correlation to prevent singular fits. Time was centered at baseline, and all continuous predictors were standardized in multivariate analysis, except for variables derived from MRI data. All models were adjusted for baseline age, sex, education level, ApoE genotype (ε4-allele carrier/non-carrier), and cognitive stage (presymptomatic, MCI, mild dementia). Linear mixed-effects models use all available data for each participant, allowing the inclusion of subjects with unequal numbers of longitudinal observations. Both, cross-sectional (biomarker as main effect) and longitudinal (biomarker × time interaction) associations were evaluated within the same model framework. P values for fixed effects were adjusted using the Benjamini–Hochberg false discovery rate (FDR) procedure, and associations with p_FDR < 0.05 were considered statistically significant. Significant biomarkers were subsequently selected as candidates for inclusion in the final multivariate model. Similarly, previous analyses were replicated using CDR-SB as the dependent variable, maintaining the same model structure and set of covariates. Since the CDR-SB variable showed positive skewness and included values close to zero, a logarithmic transformation with a unit offset (log(sumboxcdr + 1)) was applied to improve residual normality and homoscedasticity in the linear mixed models. This transformation stabilizes variance and minimizes the influence of extreme values, ensuring a more robust estimation of fixed effects and their interaction with time. Model validity was assessed by means of the distribution of simulated residuals, homoscedasticity, and the absence of systematic or hierarchical patterns indicating model misspecification, using the Kolmogorov–Smirnov, dispersion, and outliers' tests.

For each variable type (lipid peroxidation biomarkers, MRI features) and cognitive score outcome (MMSE, CDR-SB), a multivariate linear mixed-effects model was developed:

$$Y_{ij} = \beta_0 + \beta_1 Bioma\,\mathrm{ker}_i + \beta_2 Time_{ij} + \beta_3 (Bioma\,\mathrm{ker}_i * Time_{ij}) + C_i + b_{01} + b_{1i} Time_{ij} + \varepsilon_{ij}$$

where: Y_{ij} represents the cognitive score (MMSE or CDR-SB) of subject i at time j; C_i includes the fixed covariate adjustment variables; b_{0i} and b_{1i} are the random effects (intercept and slope per subject); and ε_{ij} is the residual error term.

The identification of homogeneous structural patterns among patients was performed with hierarchical clustering based on quantitative variables derived from structural MRI. The Gower distance was used as a measure of dissimilarity, and the complete linkage method was applied, given its robustness to outliers. The optimal number of clusters (k) was determined using the silhouette coefficient, selecting the value that maximized within-cluster cohesion and between-cluster separation. The hierarchical structure was visualized with a dendrogram, and patient distribution according to MRI-derived profiles was further explored using a t-SNE projection of the Gower distance matrix, allowing visualization of nonlinear relationships among observations. Subsequently, the variables with the highest discriminative contribution across clusters were evaluated using decision trees, and clinical and neuropsychological differences between groups were assessed through nonparametric tests (Kruskal–Wallis). Finally, the association between the identified clusters and longitudinal cognitive trajectories was analyzed using linear mixed-effects models, including the interaction with time to assess differential evolution in MMSE and CDR scores. Model adequacy was verified through the validation of simulated residuals, confirming the absence of systematic bias and the proper distribution of residuals. Continuous variables were described using median and interquartile range (IQR), and categorical variables were described using absolute number and percentage. Differences between groups (clusters) were analyzed using the Kruskal–Wallis test for continuous variables and Fisher's exact test for categorical variables.

R software (version 4.2.3.) was used in all the analyses[52], and the different packages were glmnet (version 4.1.7.)[53] caret (version 6.0.94)[54], cutpoint (version 1.1.2)[55] and ggplot2 (version 3.5.1)[56].

Results

Demographic and clinical description of participants

Table 1 describes the clinical and demographic data for the participants (n = 195). The mean age was 71 years, and the women represented 61% of the participants. Regarding the ApoE genotype, the percentage of ε4-allele carriers was 51.6%. Comparison of baseline characteristics between included participants and those excluded from the study (with only one available time point) revealed a significant difference in the degree of cognitive

Variable		n = 195
Sex (female) (n (%))		119 (61.0)
Age (years, median (IQR))		71.0 (67.0–74.0)
Education level (n (%))	Non-formal education	57 (29.3)
	Primary education	56 (28.7)
	Secondary education	32 (16.4)
	University education	50 (25.6)
Sum of Box CDR (score, median (IQR))		2.0 (1.5–3.5)
MMSE (score, median (IQR))		25.0 (22.0–27.0)
Cognitive impairment degree (n (%))	Preclinical	17 (8.7)
	MCI	177 (90.8)
	Mild dementia	1 (0.5)
RBANS-IM (score, median (IQR))		69.0 (53.0–81.0)
RBANS-V/C (score, median (IQR))		78.0 (66.0–89.0)
RBANS-L (score, median (IQR))		73.0 (60.0–90.0)
RBANS-A (score, median (IQR))		68.0 (56.0–85.0)
RBANS-DM (score, median (IQR))		60.0 (48.0–85.25)
FAQ (score, median (IQR))		4.0 (1.75–8.0)
ADCS-ADL-MCI (score, median (IQR))		42.0 (37.0–46.0)
GDS (score, median (IQR))		9.0 (5.75–15.0)
CSF Aβ42 (pg mL^{-1}, median (IQR))		634.0 (495.75–782.50)
CSF T-tau (pg mL^{-1}, median (IQR))		583.0 (396.75–796.25)
CSF ptau181 (pg mL^{-1}, median (IQR))		95.0 (64.0–134.25)
CSF Aβ40 (pg mL^{-1}, median (IQR))		13,834.0 (10,483.5–16,352.0)
CSF Aβ42/Aβ40 (median (IQR))		0.050 (0.042–0.057)
CSF NfL (pg mL^{-1}, median (IQR))		1010.5 (808.2–1324.7)
CSF Tau/Aβ42 (median (IQR))		0.862 (0.640–1.319)
ApoE genotype (Ɛ4-carrier, n (%))		97 (51.6)
Plasma p-Tau217 (pg mL^{-1}, median (IQR))		0.45 (0.26–0.74)

Table 1. Baseline demographic and clinical characteristics of participants. IQR: Inter-quartile range. [a] positive amyloid PET.

impairment, with a higher proportion of mild dementia among excluded patients ($p < 0.001$). Accordingly, baseline cognitive impairment degree was included as a confounding variable in the statistical models.

The individual cognitive decline trajectories were obtained from the CDR-SB and MMSE scores over time for participants with at least two time points. As expected, the trajectories for MMSE tend to decrease, while those for CDR-SB tend to increase, although some stable trajectories were observed in both cases (data not shown).

Plasma lipid peroxidation biomarkers and neuroimaging features

The plasma lipid peroxidation compound concentrations (median, inter-quartile range (IQR)) are summarized in Table 2.

The neuroimaging features obtained from the standardized scales are summarized in Table 3.

Association between multiple biomarkers and longitudinal cognitive performance

The association between different variables (plasma lipid peroxidation biomarkers, MRI features) and longitudinal cognitive decline (MMSE, CDR-SB) was evaluated.

MMSE

Regarding MMSE cognitive decline, some MRI variables were identified as significant (FDR-adjusted p-value < 0.05 in the interaction or main effect, see Table 4). However, for lipid peroxidation biomarkers, no significant variables were detected after applying correction for multiple comparisons (p_FDR < 0.05, see Table 4).

For MRI, a multivariate model was developed from the statistically significant variables previously identified. The final model was adjusted based on collinearity criteria (Variance Inflation Factor (VIF) adjusted for degrees of freedom < 2.5) and lower Akaike Information Criterion (AIC), in order to obtain a more parsimonious model (see Table 5).

This model validation was performed using simulated residuals. They showed normality ($p = 0.082$), homoscedasticity ($p = 0.700$), and conforming outliers ($p = 0.066$) without significant deviations. Also, for this model, the Root Mean Squared Error (RMSE) was 1.462, so the prediction error in the original units of the outcome could be suitable, and the conditional R^2 was 0.825, reflecting a suitable proportion of total explained variance (fixed + random effects).

Variable	Median (IQR) (nmol L^{-1}) (n = 94)
15(*R*)–15-F_{2t}-IsoP	0.00 (0.00–0.10)
PGE_2	0.00 (0.00–0.00)
2,3-dinor-15-epi-15-F_{2t}-IsoP	0.00 (0.00–0.00)
15-keto-15-E_{2t}-IsoP	1.50 (1.13–2.83)
15-keto-15-F_{2t}-IsoP	0.73 (0.53–0.94)
15-E_{2t}-IsoP	1.02 (0.36–2.11)
5-F_{2t}-IsoP	9.10 (6.06–13.54)
15-F_{2t}-IsoP	0.249 (0.246–0.252)
$PGF_{2\alpha}$	0.00 (0.00–0.00)
1a,1b-dihomo-$PGF_{2\alpha}$	0.00 (0.00–0.00)
Neuroprostanes [a]	0.09 (0.07–0.12)
Isoprostanes [a]	0.84 (0.65–1.08)
Neurofurans [a]	0.05 (0.03–0.08)
Isofurans [a]	0.32 (0.25–0.41)
DihomoIsoprostanes [a]	0.62 (0.57–0.70)
DihomoIsofurans [a]	0.19 (0.15–0.22)

Table 2. Concentrations found for lipid peroxidation compounds in plasma samples from the participants. [a] Total parameters, expressed as arbitrary units: (intensity of signal units × (internal standard concentration, nmol L^{-1}).

CDR sum of boxes

Regarding CDR-SB cognitive decline, some MRI variables were detected as significant (FDR-adjusted p value < 0.05) (in the interaction or main effect, see Table 6). However, for lipid peroxidation biomarkers, no significant variables were detected after applying correction for multiple comparisons (p_FDR < 0.05, see Table 6).

For MRI, a multivariate model was developed from the statistically significant variables previously identified. The final model was adjusted based on collinearity criteria (Variance Inflation Factor (VIF) adjusted for degrees of freedom < 2.5) and lower AIC (Akaike Information Criterion), in order to obtain a more parsimonious model (see Table 7).

This model validation was performed using simulated residuals. They showed normality (p = 0.746), homoscedasticity (p = 0.928), and conforming outliers (p = 0.057) without significant deviations. The MRI multivariate model showed a RMSE of 0.202, and a conditional R^2 of 0.808, reflecting a relevant and explanatory contribution.

Hierarchical clustering of patients

A hierarchical clustering was performed based on quantitative variables derived from MRI. The optimal number of clusters was determined through silhouette coefficient analysis, selecting the k value that maximized internal cohesion and separation between groups. The optimal k according to the silhouette was 4. The number of patients were cluster 1 (n = 62), cluster 2 (n = 57), cluster 3 (n = 34), cluster 4 (n = 13).

The distribution of patients according to their MRI profiles was additionally visualized through a t-distributed stochastic neighbor embedding (t-SNE) projection applied to the Gower distance matrix, which allowed exploration of the non-linear relationship between observations (see Fig. 2).

The hierarchical clustering analysis, performed using Gower distance, revealed a clustering structure composed of k = 4 optimal groups according to the average silhouette coefficient (0.265). The t-SNE projection showed clear visual differentiation among most clusters, with slight interlacing of group 4 between two of them. Overall, these results indicate the existence of a latent structure in the data, with some partial overlap between adjacent groups but consistent global separation.

To facilitate the clustering structure interpretation, a decision tree classifier was fitted from the same input variables (see Fig. 3). Its complexity was deliberately constrained to yield a simple structure and avoid excessively detailed data partitioning.

The upper levels of the tree identify the Koedam score (left hemisphere) as the primary variable driving cluster separation. Patients with lower values are predominantly assigned to cluster 1, indicating a distinct profile. Among the remaining cases, cortical volumetric measures (EPV_cortical) further separate a well-defined group corresponding to cluster 2. The subsequent splits contribute distinguishing the remaining patients, although with less clear separation, reflecting greater overlap between clusters. Overall, the tree highlights a small set of variables with strong discriminative capacity at the top of the hierarchy, followed by more nuanced partitioning at deeper levels.

MRI and cognitive decline differences among clusters were described (see Table 8). From the slopes of cognitive decline, it was observed that cluster 4 showed lower values for CDR-SB slope and MMSE slope; therefore, it may be considered the group with the most favourable AD progression. Statistically significant differences were found for all the MRI variables and MMSE slope among clusters.

Variable		n (%) (n = 178)
Scheltens Right[49]	0	42 (25.00)
	1	63 (37.50)
	2	46 (27.38)
	3	13 (7.74)
	4	4 (2.38)
Scheltens Left[49]	0	59 (35.12)
	1	52 (30.95)
	2	40 (23.81)
	3	14 (8.33)
	4	3 (1.79)
Koedam Right[50]	0	68 (38.20)
	1	63 (35.39)
	2	43 (24.16)
	3	4 (2.25)
Koedam Left[50]	0	68 (38.20)
	1	62 (34.83
	2	42 (23.60)
	3	6 (3.37)
Fazekas[51]	0	45 (25.28)
	1	90 (50.56)
	2	36 (20.22)
	3	7 (3.93)
Microhemorrhages	0	146 (83.43)
	1	19 (10.86)
	2	7 (4.00)
	3	3 (1.71)
EPV BBGG	0	88 (49.44)
	1	66 (38.76)
	2	23 (12.92)
	3	1 (0.56)
EPV cortical	0	90 (50.56)
	1	69 (38.76)
	2	19 (10.67)
EPV midbrain	0	138 (77.53)
	1	30 (16.85)
	2	10 (5.62)
EPV temporoinsular region	0	114 (64.04)
	1	61 (34.27)
	2	3 (1.69)

Table 3. Neuroimaging features obtained from the scans of the participants. Microhemorrhages: 0 = 0 microbleeds; 1 = 1–2 microbleeds; 2 = 3–10 microbleeds; 3 = > 10 microbleeds. BBGG: Basal Ganglia. EPV: enhanced perivascular spaces: 0 = absent; 1 = 1–2 mm; 2 = 2–4 mm; 3 = > 4 mm.

A linear mixed model was fitted to evaluate the evolution of cognitive performance (MMSE) over time, considering membership in the different clusters and adjusting for relevant demographic and genetic covariates. Random intercepts and slopes per subject were included to capture interindividual variability in both initial level and rate of temporal change. The results for MMSE are summarized in Table 9.

This model validation was performed using simulated residuals. They showed normality ($p = 0.105$), homoscedasticity ($p = 0.486$) and conforming outliers ($p = 0.120$), without significant deviations. Clusters 2 and 3 showed significantly lower initial scores than the reference group (Cluster 4), $\beta = -3.26$ ($p = 0.021$) and $\beta = -3.54$ ($p = 0.017$), respectively. This indicates that these groups start with lower cognitive performance, compatible with a more deteriorated profile or with greater clinical/biological burden. Cluster 1 did not differ significantly from the reference group ($\beta = -1.17$, $p = 0.41$), suggesting comparable initial cognitive performance. The Time:Cluster interactions did not reach statistical significance ($p > 0.12$), although the negative coefficients for Clusters 2 and 3 (≈ -0.9) suggest a possible trend toward more pronounced decline in these groups. The lack of significance may be due to high interindividual variability or insufficient temporal follow-up.

Variable	Term	Effect size (β coefficient)	Standard error	P value	p-FDR
Scheltens Left	Interaction	−0.643	0.141	0.00001	0.00009***
Scheltens Right	Interaction	−0.545	0.147	0.0003	0.0012 ***
Scheltens Left	Main	−1.328	0.309	0.00003	0.0002***
Koedam Right	Main	−1.352	0.346	0.0001	0.0003***
Koedam Left	Main	−1.320	0.337	0.0001	0.0003 ***
Scheltens Right	Main	−1.0612014	0.3311876	0.0016	0.003 **
8-iso-PGF2α	Interaction	0.355	0.168	0.041	0.337
IsoF tot	Main	0.970	0.460	0.037	0.210
8-iso-15-keto-PGF2α	Main	0.986	0.468	0.038	0.210

Table 4. Univariate association between MMSE cognitive decline over time and MRI features or plasma lipid peroxidation compounds. *** $p < 0.001$, ** $p < 0.01$, * $p < 0.05$.

Fixed effects	Effect size (β coefficient)	Standard error	P value
Intercept	26.63246	4.20685	2.14e-09***
Scheltens Left	−1.06516	0.31784	0.000976***
Time	−0.69624	0.19521	0.000510***
Koedam Left	−0.96475	0.34613	0.005924**
Age	0.03517	0.05459	0.520312
Sex	−2.07327	0.61612	0.000946***
Education level	0.66011	0.26036	0.012141*
ApoE genotype	0.63486	0.57817	0.273728
MCI level	−4.93819	1.11930	1.88e-5***
Mild dementia level	−14.39061	4.46191	0.001420**
Scheltens Left : Time	−0.63995	0.14136	1.17e-5***

Table 5. Fixed effects coefficients of the multivariate model including significant MRI variables. *** $p < 0.001$, ** $p < 0.01$, * $p < 0.05$.

Variable	Term	Effect size (β coefficient)	standard error	P value	p_FDR
Scheltens Left	Interaction	0.047	0.016	4.858 e-3	0.0389 *
Scheltens Left	Main	0.157	0.034	8.349 e-6	0.00007***
Scheltens Right	Main	0.154	0.036	2.994 e-5	0.00012 ***
Koedam Right	Main	0.107	0.039	7.157 e-3	0.017 *
Koedam Left	Main	0.103	0.038	8.370 e-3	0.017*
Isofurans	main	−0.117	0.047	0.014	0.159

Table 6. Univariate association between CDR-SB cognitive decline over time and MRI features or plasma lipid peroxidation compounds. *** $p < 0.001$, ** $p < 0.01$, * $p < 0.05$.

The model for CDR-SB was fitted to evaluate the evolution of cognitive performance (log(sumboxcdr + 1)) over time, considering membership in the different clusters and adjusting for relevant demographic covariates. Random intercepts and slopes per subject were included to capture interindividual variability in both initial level and rate of temporal change (see Table 10).

This model validation was performed using simulated residuals. They showed normality ($p = 0.230$), homoscedasticity ($p = 0.768$) and conforming outliers ($p = 1.000$) without significant deviations. Cluster 2 showed a marginal trend toward presenting higher initial values of log(CDR + 1) compared to the reference group (Cluster 4) ($\beta = 0.28$, $p = 0.077$), suggesting a greater degree of baseline clinical deterioration in this group. Cluster 3 showed a slight non-significant increase ($\beta = 0.21$, $p = 0.21$), while Cluster 1 did not differ from the reference group ($\beta = 0.11$, $p = 0.50$). Overall, these results suggest that only Cluster 2 might represent an initially more advanced clinical profile, although the statistical evidence is limited ($p \approx 0.08$).

Discussion

This biennial follow-up study of early AD patients consisted of the assessment of cognitive decline trajectories (MMSE, CDR-SB) using lipid peroxidation compounds and MRI features. The results showed that MRI biomarkers exhibited robust associations with both MMSE and CDR-SB tests, while plasma lipid peroxidation

Fixed effects	Effect size (β coefficient)	Standard error	P value
Intercept	0.463	0.483	0.339
Scaled Scheltens Left	0.158	0.034	8.35 e-6***
Time	0.176	0.016	< 2e-16***
Age	−0.0011	0.006	0.858
Sex	0.118	0.070	0.092
Education level	−0.053	0.029	0.072
ApoE genotype	−0.031	0.065	0.631
MCI level	1.090	0.127	8.86 e-15***
Mild dementia level	1.677	0.508	0.0011**
Scaled Scheltens Left: Time	0.0470	0.016	0.0049**

Table 7. Fixed effects coefficients of the multivariate model including significant MRI variables. *** $p < 0.001$, ** $p < 0.01$, * $p < 0.05$.

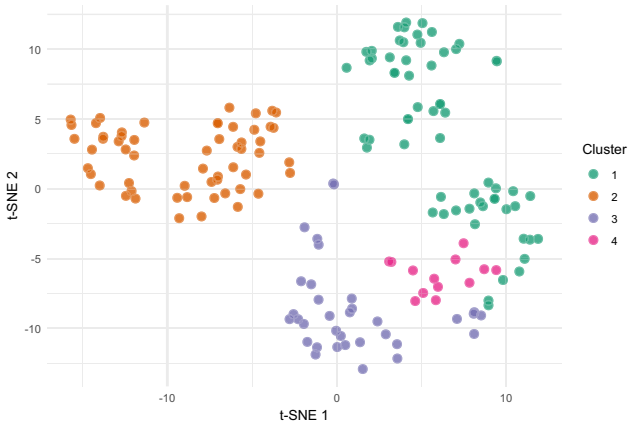

Fig. 2. t-SNE projection based on the Gower distance matrix. Points represent patients and are coloured by hierarchical clustering groups (k = 4). Axes correspond to the two-dimensional embedding; shorter distances reflect higher similarity between MRI profiles.

biomarkers did not achieve statistical significance, suggesting that peripheral oxidative stress biomarkers may have limited utility as prognostic indicators of cognitive decline. For MRI features, hierarchical clusters identified four distinct patient subgroups, demonstrating significant disease heterogeneity. The corresponding decision tree provided an interpretable approximation of the clustering structure, highlighting the main variables contributing to subgroup differentiation, and the mixed-effects models including cluster membership showed significant baseline differences in MMSE, with lower initial scores in clusters 2 and 3, while for CDR-SB only a marginal increase at baseline was observed in cluster 2. No significant differences were found in longitudinal trajectories in either model, although the coefficients suggested a tendency toward greater decline for MMSE in clusters 2 and 3.

Several studies have examined the role and activity of potential oxidative stress biomarkers. For instance, Zhang et al[57]. examined the involvement of nitric oxide, demonstrating that endothelial nitric oxide synthase (eNOS) inactivation may lead to significant cognitive impairment. Other research has focused on identifying genes modified or associated with oxidative stress[58,59]. However, some oxidative stress biomarkers show limited specificity for AD pathology[60]. For lipid peroxidation biomarkers, a previous study showed that their plasma levels were impaired at early AD stages[61], constituting promising biomarkers for early AD diagnosis. Also, some plasma lipid peroxidation compounds were identified as useful progression AD biomarkers[62], since they showed an increasing trend over time. Moreover, some studies have increasingly shifted toward other plasma biomarkers like NfL, GFAP, the Aβ42/Aβ40 ratio, p-Tau181[63,64], as well as p-Tau231 and p-Tau217[65], which exhibit stronger associations with disease progression risk. Prognostic studies in AD evaluated the conversion from MCI to dementia. Evidence from Honey et al[66]. highlights the prognostic value of plasma biomarkers (p-Tau217, p-Tau181, NfL, GFAP) for predicting dementia onset in individuals without dementia. Their findings from the Amsterdam Dementia Cohort demonstrate that these biomarkers can reliably predict clinical progression to dementia. The divergence from our plasma lipid peroxidation biomarkers, which did not reach statistical significance, underscores that not all peripheral biomarkers offer equivalent prognostic utility for predicting cognitive decline. In recent literature, the peripheral biomarkers showed limited differential sensitivity across AD stages compared to neuroimaging[67,68].

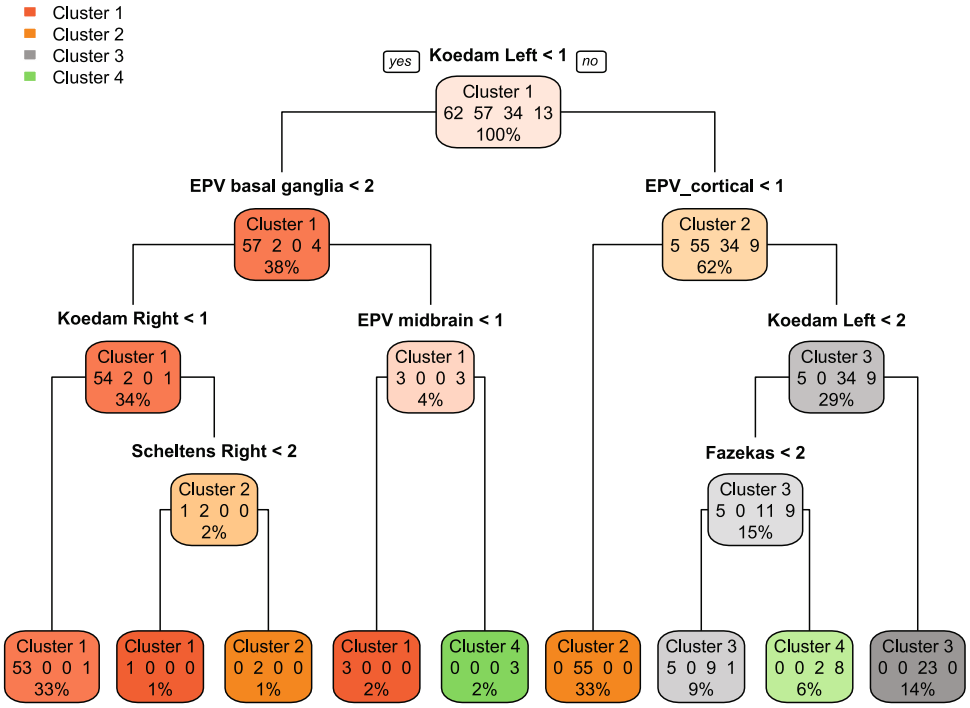

Fig. 3. Decision tree approximating cluster membership from MRI-derived features. Each node shows the predicted cluster (first line), the distribution of subjects to each cluster within the subgroup (second line), and the percentage of the total samples included in the subgroup (third line). Node color encodes the predicted cluster, using darker tones to reflect higher class probability in the node. The hierarchical structure illustrates how a reduced set of variables contributes to the separation of patients groups.

Variable		Median (IQR)				Kruskal–Wallis P Value
		Cluster 1	Cluster 2	Cluster 3	Cluster 4	
Scheltens Right		1.0 (0.0–1.0)	1.0 (1.0–2.0)	2.0 (1.0–2.0)	2.0 (2.0–3.0)	< 0.0001
Scheltens Left		0.0 (0.0–1.0)	1.0 (1.0–2.0)	2.0 (1.0–2.0)	2.0 (1.0–2.0)	< 0.0001
Koedam Right		0.0 (0.0–0.0)	1.0 (1.0–2.0)	2.0 (1.0–2.0)	0.0 (0.0–1.0)	< 0.0001
Koedam Left		0.0 (0.0–0.0)	1.0 (1.0–2.0)	2.0 (1.0–2.0)	1.0 (0.0–1.0)	< 0.0001
Fazekas		1.0 (0.0–1.0)	1.0 (0.0–1.0)	1.0 (1.0–1.8)	2.0 (2.0–2.0)	< 0.0001
Microhemorrhages		0.0 (0.0–0.0)	0.0 (0.0–0.0)	0.0 (0.0–0.0)	0.0 (0.0–1.0)	0.0337
EPV basal ganglia		1.0 (0.0–1.0)	0.0 (0.0–0.0)	1.0 (1.0–2.0)	2.0 (1.0–2.0)	< 0.0001
EPV cortical		1.0 (0.0–1.0)	0.0 (0.0–0.0)	1.0 (1.0–1.0)	1.0 (1.0–2.0)	< 0.0001
EPV midbrain		0.0 (0.0–0.0)	0.0 (0.0–0.0)	0.0 (0.0–1.0)	1.0 (1.0–1.0)	< 0.0001
EPV temporoinsular region		0.0 (0.0–1.0)	0.0 (0.0–0.0)	1.0 (0.0–1.0)	1.0 (1.0–1.0)	< 0.0001
CDR slope		0.5 (0.2–1.1)	0.9 (0.3–1.9)	0.8 (−0.1–1.7)	0.2 (0.0–0.4)	0.1193
MMSE slope		−0.4 (−1.7–0.4)	−1.5 (−2.9–0.0)	−1.2 (−2.3–0.0)	0.0 (−0.4–0.0)	< 0.05
Baseline MMSE		26.0 (23.0- 28.0)	25.0 (21.0-, 27.0)	23.5 (20.0- 26.0)	25.0 (25.0- 27.0)	0.065
Baseline CDR-SB		2.0 (1.0–3.0)	2.5 (1.5–3.5)	3.0 (1.5–3.5)	1.5 (1.5–3.0)	0.128
Sex (n (%))	Women	44 (45)	31 (32)	19 (19)	4 (4)	0.032
	Men	18 (26)	26 (38)	15 (22)	9 (13)	
Age		71.0 (66.5, 73.0)	71.0 (68.0, 73.0)	73 (70.2, 74.0)	73.0 (71.0, 74.0)	0.078
Education level (n (%))	Basic	17 (36)	13 (28)	12 (25)	5 (11)	0.812
	Primary	18 (37)	16 (33)	10 (21)	4 (8)	
	Secondary	11 (42)	10 (38)	5 (19)	0 (0)	
	University	16 (36)	18 (40)	7 (16)	4 (9)	
ApoE genotype (n (%)) (Ɛ4-carrier)		30 (38)	26 (33)	18 (23)	4 (5)	0.586

Table 8. Description of MRI and clinical progression variables among the identified clusters. IQR: Inter-quartile range.

	Effect size (β coefficient)	Standard error	P value
Intercept	28.511	5.221	2.36e-7***
Time	−0.604	0.544	0.270
Cluster1	−1.172	1.408	0.407
Cluster 2	−3.263	1.392	0.021*
Cluster 3	−3.544	1.465	0.017*
Age	0.012	0.066	0.856
Sex	−1.713	0.739	0.022*
Education level	0.748	0.300	0.014*
ApoE genotype	0.703	0.675	0.300
MCI level	−5.214	1.200	2.79e-5***
Time:cluster1	−0.356	0.600	0.552
Time:cluster 2	−0.935	0.606	0.126
Time:cluster 3	−0.920	0.633	0.149

Table 9. Coefficients of the multivariate model for MMSE evolution including clusters and demographic variables. *** $p < 0.001$, ** $p < 0.01$, * $p < 0.05$.

	Effect size (β coefficient)	Standard error	P value
Intercept	−0.186	0.590	0.752
Time	0.101	0.062	0.108
Cluster1	0.107	0.158	0.499
Cluster 2	0.279	0.156	0.077
Cluster 3	0.208	0.164	0.209
Age	0.004	0.007	0.621
Sex	0.141	0.083	0.092
Education level	−0.051	0.034	0.134
ApoE genotype	−0.022	0.076	0.769
MCI level	1.214	0.135	2.67e-15***
Time:cluster1	0.075	0.068	0.276
Time:cluster 2	0.097	0.069	0.165
Time:cluster 3	0.052	0.072	0.470

Table 10. Coefficients of the multivariate model for CDR-SB evolution including clusters and demographic variables. *** $p < 0.001$, ** $p < 0.01$, * $p < 0.05$.

Regarding MRI, the present study showed a notable prognostic predictive capacity of the features obtained from visual scales. Specifically, the Scheltens scale, which assesses bilateral medial temporal atrophy; and the Koedam scale, which assesses bilateral posterior atrophy, showed significant associations with cognitive trajectories. Multivariate models incorporating these MRI measures showed strong prognostic performance and low prediction errors for both MMSE and CDR-SB. For MMSE, the linear mixed model showed a significant effect of the biomarker in the main term (Scheltens Left, Koedam Left), indicating a cross-sectional association between biomarker levels and cognitive function, reflecting differences in baseline or average performance across individuals throughout follow-up. In contrast, a significant effect in the biomarker × time interaction (Scheltens Left:Time) suggested that this biomarker modulated the slope of cognitive change, that is, the rate of deterioration or stability over time. For CDR-SB, the linear mixed model showed significant effects of the Scheltens Left in the main term and in the biomarker × time interaction. Thus, biomarkers with significance only in the main term are associated with baseline cognitive level, while those with a significant interaction predict differential progression trajectories, regardless of baseline status. In this case, both effects were significant, therefore Scheltens Left was associated with both baseline cognitive level and rate of change (MMSE, CDR-SB), providing a more complete prognostic value of cognitive decline. These results indicate that structural MRI patterns effectively capture baseline cognitive impairment as well as inter-individual differences in progression rates. Similarly, a previous study[69] analyzed the cognitive decline rate (slow and fast), showing that at baseline there were no differences in demographics, MMSE, vascular burden, or medial temporal lobe atrophy measurements. However, it identified a fast-progressor group (≥3 MMSE points decline/year)[69], characterized by elevated plasma NfL and lower baseline MMSE, with high specificity.

The AD heterogeneity has been largely evaluated to identify different AD subtypes. In the present study it was evaluated the variability of the disease progression (rate, trajectory) through cluster analysis from quantitative MRI variables, identifying four subgroups, which were visualized by a decision tree. They showed different neuroimaging and cognitive decline profiles; cluster 1 exhibited minimal atrophy across all regions; clusters

2 and 3 exhibited the greatest posterior cortical atrophy, with cluster 2 demonstrating fast-cognitive decline; and cluster 4 showed the most severe medial temporal atrophy, white matter disease, and enlarged perivascular spaces but remained cognitively stable. Similarly, a previous study[70] identified different prognostic subtypes (low, mild and fast) using 3D MRI combined with cognitive and genetic indicators. In the present work, all MRI features and MMSE slope showed statistically significant differences among clusters, indicating that they could represent distinct pathological phenotypes with different MMSE cognitive progression. In this sense, a previous work studying 14 brain regions of interest with MRI images (1.5 T, 3.0 T MRI, and T1-weighted MRI) showed that several AD subtypes exist[71]. They are typical (early hippocampal and amygdala atrophy representing classic Alzheimer's pathology), subcortical (hippocampal-sparing variant with subtle subcortical atrophy), and cortical subtype (early insula and cingulate atrophy). Interestingly, a relationship between these subtypes and the four subtypes identified in the present study can be inferred from their distinct neuroanatomical and clinical patterns. First, the typical subtype, characterized by an early hippocampal and amygdala atrophy, would correspond to clusters 3 and 4 in the present work, showing the highest Scheltens scores (medial temporal lobe atrophy). However, cluster 3 showed moderate cognitive decline (MMSE), while cluster 4 remained cognitively stable. This could be explained by the different stages of the typical AD progression or the cognitive reserve in cluster 4. Second, the cortical subtype, featuring early insula and cingulate atrophy, would align with clusters 2 and 3, showing the highest Koedam scores (posterior cortical atrophy). However, cluster 2 showed the fast-cognitive decline with minimal hippocampal involvement, representing a purer cortical-predominant variant; while cluster 3 showed a mixed phenotype with both hippocampal and cortical atrophy, explaining its intermediate cognitive decline pattern. Third, the subcortical or hippocampal-sparing subtype would correspond to cluster 4, which paradoxically showed high Scheltens scores but maintained cognitive stability. This cluster exhibited the most severe white matter disease as it can be seen in Fazekas score, and extensive perivascular spaces across all regions (basal ganglia, cortical, midbrain, temporoinsular), suggesting predominant subcortical vascular pathology or concomitant MCI due to cerebrovascular disease. The cognitive stability despite structural changes supports the hippocampal-sparing concept and may explain why this subtype includes a higher proportion of control subjects. Finally, cluster 1 exhibited minimal atrophy across all measures, probably reflecting early-stage disease, prodromal presentations, or a resilient phenotype that did not fit into previously established subtypes. The individuals in this cluster may possess high cognitive reserve, or they may represent a preclinical stage at which subtype-specific differentiation has yet to emerge. Furthermore, according to the established AD subtypes described by Ferreira et al.[26], the clusters identified in the present study may be aligned as follows: cluster 3 with the typical subtype, since it exhibited high temporal and cortical atrophy; cluster 2 with the hippocampal-sparing subtype, showing greater posterior cortical atrophy and relative hippocampal preservation; cluster 4 with the limbic-predominant subtype, showing greater medial temporal atrophy and higher vascular burden; and cluster 1 with the minimal atrophy subtype, given its overall lower degree of atrophy.

In general, these four identified clusters reflect the heterogeneity of AD progression. The identification of these subgroups may improve personalized prognostic assessment and clinical management. In fact, clusters 2 and 3 exhibited a more rapid cognitive decline compared to clusters 1 and 4. However, cluster 4 was expected to exhibit a worst prognosis, given the presence of vascular pathology (Fazekas and EPVS scores), and as well as medial temporal atrophy. This observation may be influenced by the small sample size in this cluster. Therefore, further validation in larger cohorts is required prior to clinical implementation. In addition, it is important to highlight that structural atrophy (local and global) could be related to disruptions in large-scale brain network organization[72]. In fact, a progressive degeneration and loss of white and grey matter, may drive to an extensive disconnection between brain regions, leading to alterations in functional connectivity.

The AD prognosis prediction was evaluated by considering membership in the different previously identified clusters and adjusting for relevant demographic and genetic covariates. The developed model for MMSE showed that two clusters exhibited significantly lower baseline MMSE scores, compatible with a more deteriorated profile or with greater clinical/biological burden, but the rates of decline (Time:Cluster interactions) did not differ significantly across groups. However, the negative coefficients for these clusters (2, 3) may suggest a possible trend toward more pronounced decline in these groups. The lack of significance may be due to high interindividual variability or insufficient temporal follow-up. Overall, the model suggests that membership in certain clusters (2, 3) is associated with worse initial cognitive performance, even after adjusting for age, sex, education, and clinical status. Although differences in temporal slope did not reach significance, the coefficients point to a possible acceleration of deterioration in these groups, which could reflect underlying biological or phenotypic differences between clusters. Notably, another cluster exhibited the highest vascular pathology burden yet demonstrated the slowest cognitive decline, suggesting that neurodegenerative and cerebrovascular mechanisms may confer differential prognostic. The developed model for CDR-SB showed that cluster 2 exhibited a marginal trend toward presenting higher initial values for CDR-SB compared to the reference group, suggesting a greater degree of baseline clinical deterioration or a more advanced clinical profile in this group.

Some limitations of this study should be acknowledged. First, loss to follow-up was observed over time, and patients with only one available assessment were excluded from this study. It was mainly related to disease progression, including death and severe cognitive deterioration. However, comparing baseline characteristics between included and excluded participants, only a significant difference in the degree of cognitive impairment was observed; so, this information was included as a confounding variable. Moreover, some patients had a relatively short follow-up. This non-random attrition may have led to an underrepresentation of rapidly progressive trajectories at later assessments. However, such patterns are inherent to longitudinal studies in AD and reflect its natural course. In addition, to mitigate potential selection bias with both longitudinal attrition and exclusion, relevant baseline characteristics, including cognitive impairment degree, were incorporated as confounding variables in the statistical models. Second, the sample size for plasma lipid peroxidation analysis (n = 94) was smaller than that of the full cohort (n = 226), which may have limited statistical power to detect

significant associations with cognitive decline. Third, the number of patients with ≥ 3 measures of MMSE or CDR-SB was lower than the total cohort, potentially affecting the detection of temporal relationships. Finally, the visual assessment of MRI may be less sensitive than volumetric analysis, but is simplicity makes it more feasible for routine clinical implementation. In addition, the longitudinal design allowed the characterization of distinct cognitive decline trajectories using robust analytical approaches. The well-characterized cohort and extended follow-up further support the validity of the results and their contribution to understanding heterogeneity in AD progression.

Conclusion

Longitudinal assessment of cognitive decline in early AD revealed significant associations with the MRI features obtained from standardized visual scales (Scheltens Left and Right scores, Koedam Left and Right scores), whereas plasma lipid peroxidation biomarkers showed no significant relationship. From these MRI variables, cluster analysis identified four distinct clinical profiles, likely corresponding to typical, subcortical and cortical subtypes, each showing different cognitive decline trajectories. Therefore, predictive models incorporating cluster membership improved prognostic classification. For MMSE, two clusters showed higher baseline cognitive impairment, while another cluster showed intermediate values without significant differences compared to the reference cluster. Overall, these findings suggest that MRI-based stratification captures clinical subgroups with different degrees of impairment and patterns of disease progression, supporting its utility for prognosis in early AD.

Data availability

Data are available upon request to the corresponding author.

Received: 21 May 2026; Accepted: 24 June 2026
Published online: 26 June 2026

References

1. Graff-Radford, J. et al. New insights into atypical Alzheimer's disease in the era of biomarkers. *Lancet Neurol.* **20**, 222–234. https://doi.org/10.1016/S1474-4422(20)30440-3 (2021).
2. Kim, K. Y., Shin, K. Y. & Chang, K. A. GFAP as a potential biomarker for Alzheimer's disease: A systematic review and meta-analysis. *Cells* **12**, 1309. https://doi.org/10.3390/cells12091309 (2023).
3. Wojdała, A. L. et al. Trajectories of CSF and plasma biomarkers across Alzheimer's disease continuum: disease staging by NF-L, p-tau181, and GFAP. *Neurobiol. Dis.* **189**, 106356. https://doi.org/10.1016/j.nbd.2023.106356 (2023).
4. Leuzy, A. et al. Considerations in the clinical use of amyloid PET and CSF biomarkers for Alzheimer's disease. *Alzheimers Dement.* **21**, e14528. https://doi.org/10.1002/alz.14528 (2025).
5. Jack, C. R. Jr. et al. Revised criteria for diagnosis and staging of Alzheimer's disease: Alzheimer's Association Workgroup. *Alzheimers Dement.* **20**, 5143–5169. https://doi.org/10.1002/alz.13859 (2024).
6. Völgyi, K. et al. Mitochondrial proteome changes correlating with β-amyloid accumulation. *Mol. Neurobiol.* **54**, 2060–2078. https://doi.org/10.1007/s12035-015-9682-4 (2017).
7. Öksüz, N., Ghouri, R., Taşdelen, B., Uludüz, D. & Özge, A. Mild cognitive impairment progression and Alzheimer's disease risk: A comprehensive analysis of 3553 cases over 203 months. *J. Clin. Med.* **13**, 518. https://doi.org/10.3390/jcm13020518 (2024).
8. Cho, S. H. et al. Disease progression modelling from preclinical Alzheimer's disease (AD) to AD dementia. *Sci. Rep.* **11**, 4168. https://doi.org/10.1038/s41598-021-83585-3 (2021).
9. Li, K., Chan, W., Doody, R. S., Quinn, J. & Luo, S. Prediction of conversion to Alzheimer's disease with longitudinal measures and time-to-event data. *J. Alzheimers Dis.* **58**, 361–371. https://doi.org/10.3233/JAD-161201 (2017).
10. van der Veere, P. J. et al. Predicting cognitive decline in amyloid-positive patients with mild cognitive impairment or mild dementia. *Neurology* **103**, e209605. https://doi.org/10.1212/WNL.0000000000209605 (2024).
11. Hughes, C. P., Berg, L., Danziger, W. L., Coben, L. A. & Martin, R. L. A new clinical scale for the staging of dementia. *Br. J. Psychiatry* **140**, 566–572. https://doi.org/10.1192/bjp.140.6.566 (1982).
12. Randolph, C., Tierney, M. C., Mohr, E. & Chase, T. N. The Repeatable Battery for the Assessment of Neuropsychological Status (RBANS): Preliminary clinical validity. *J. Clin. Exp. Neuropsychol.* **20**, 310–319. https://doi.org/10.1076/jcen.20.3.310.823 (1998).
13. Alvarez-Sanchez, L. et al. Fast declining prediction in Alzheimer's disease from early clinical assessment. *Curr. Neuropharmacol.* **23**, 602–611. https://doi.org/10.2174/011570159X332930240925095423 (2025).
14. Clemmensen, F. K. et al. Prognostic value of plasma biomarkers in early Alzheimer's disease: a longitudinal clinical and neuroimaging study. *Alzheimers Res. Ther.* **17**, 243. https://doi.org/10.1186/s13195-025-01892-7 (2025).
15. Ingannato, A. et al. Plasma GFAP NfL and pTau 181 detect preclinical stages of dementia. *Front. Endocrinol. (Lausanne)* **15**, 1375302. https://doi.org/10.3389/fendo.2024.1375302 (2024).
16. Chu, C. et al. Development and validation of an interpretable clinical scoring model to monitor the progression of preclinical Alzheimer's disease. *Alzheimers Res. Ther.* **17**, 268. https://doi.org/10.1186/s13195-025-01931-3 (2025).
17. Di Domenico, F., Coccia, R., Butterfield, D. A. & Perluigi, M. Circulating biomarkers of protein oxidation for Alzheimer disease: Expectations within limits. *Biochim. Biophys. Acta* **1814**, 1785–1795. https://doi.org/10.1016/j.bbapap.2011.10.001 (2011).
18. Martí Navia, A. et al. Adenosine receptors as neuroinflammation modulators: role of A1 agonists and A2A antagonists. *Cells* **9**, 1739. https://doi.org/10.3390/cells9071739 (2020).
19. Perluigi, M., Di Domenico, F. & Butterfield, D. A. Oxidative damage in neurodegeneration: Roles in the pathogenesis and progression of Alzheimer disease. *Physiol. Rev.* **104**, 103–197. https://doi.org/10.1152/physrev.00030.2022 (2024).
20. Di Domenico, F., Barone, E., Perluigi, M. & Butterfield, D. A. The triangle of death in Alzheimer's disease brain: The aberrant cross-talk among energy metabolism, mammalian target of rapamycin signaling, and protein homeostasis revealed by redox proteomics. *Antioxid. Redox Signal.* **26**, 364–387. https://doi.org/10.1089/ars.2016.6759 (2017).
21. Gong, Z. et al. Early axonal degeneration linked to clinical decline in Alzheimer's disease progression revealed with diffusion MRI. *J. Clin. Invest.* **136**, e196638. https://doi.org/10.1172/JCI196638 (2025).
22. Mulumba, J. et al. The role of neuroimaging in Alzheimer's disease: implications for the diagnosis, monitoring disease progression, and treatment. *Explor. Neurosci.* **4**, 100675. https://doi.org/10.37349/en.2025.100675 (2025).
23. He, H. et al. Free-water imaging predicts cognitive decline and clinical progression in cognitively normal older adults. *J. Affect. Disord.* **398**, 121108. https://doi.org/10.1016/j.jad.2025.121108 (2026).
24. García-Gutiérrez, F., Matias-Guiu, J. A. & Ayala, J. L. Deep multimodal learning for domain-level cognitive decline prediction in Alzheimer's disease. *Front. Artif. Intell.* **8**, 1731062. https://doi.org/10.3389/frai.2025.1731062 (2025).

25. Prosser, L. et al. Biomarker pathway heterogeneity of amyloid-positive individuals. *Alzheimers Dement.* **20**, 8503–8515. https://doi.org/10.1002/alz.14287 (2024).
26. Ferreira, D., Nordberg, A. & Westman, E. Biological subtypes of Alzheimer disease: A systematic review and meta-analysis. *Neurology* **94**, 436–448. https://doi.org/10.1212/WNL.0000000000009058 (2020).
27. Petersen, C. et al. Alzheimer's disease clinical variants show distinct regional patterns of neurofibrillary tangle accumulation. *Acta Neuropathol.* **138**, 597–612. https://doi.org/10.1007/s00401-019-02036-6 (2019).
28. Polsinelli, A. J. & Apostolova, L. G. Atypical Alzheimer disease variants. *Continuum (Minneap. Minn.)* **28**, 676–701. https://doi.org/10.1212/CON.0000000000001082 (2022).
29. Woo, M. S. et al. Identification of late-stage tau accumulation using plasma phospho-tau217. *EBioMedicine* **109**, 105413. https://doi.org/10.1016/j.ebiom.2024.105413 (2024).
30. Ferré-González, L., Peña-Bautista, C., Baquero, M. & Cháfer-Pericás, C. Assessment of lipid peroxidation in Alzheimer's disease differential diagnosis and prognosis. *Antioxidants (Basel)* **11**, 551. https://doi.org/10.3390/antiox11030551 (2022).
31. Yu, X. et al. Innovative multivariable model combining MRI radiomics and plasma indexes predicts Alzheimer's disease conversion: Evidence from a 2-cohort longitudinal study. *Research (Wash. D.C.)* **7**, 0354. https://doi.org/10.34133/research.0354 (2024).
32. Xie, L. et al. Baseline structural MRI and plasma biomarkers predict longitudinal structural atrophy and cognitive decline in early Alzheimer's disease. *Alzheimers Res. Ther.* **15**, 79. https://doi.org/10.1186/s13195-023-01210-z (2023).
33. Göschel, L. et al. Plasma p-tau181 and GFAP reflect 7T MR-derived changes in Alzheimer's disease: a longitudinal study of structural and functional MRI and MRS. *Alzheimers Dement.* **20**, 8684–8699. https://doi.org/10.1002/alz.14318 (2024).
34. Bluma, M. et al. Disentangling relationships between Alzheimer's disease plasma biomarkers and established biomarkers in patients of tertiary memory clinics. *EBioMedicine* **112**, 105504. https://doi.org/10.1016/j.ebiom.2024.105504 (2025).
35. Palmqvist, S. et al. Prediction of future Alzheimer's disease dementia using plasma phospho-tau combined with other accessible measures. *Nat. Med.* **27**, 1034–1042. https://doi.org/10.1038/s41591-021-01348-z (2021).
36. Peña-Bautista, C. et al. Clinical usefulness of cerebrospinal fluid biomarkers in Alzheimer's disease. *Eur. J. Clin. Invest.* **53**, e13910. https://doi.org/10.1111/eci.13910 (2023).
37. Jack, C. R. Jr. et al. NIA-AA Research Framework: toward a biological definition of Alzheimer's disease. *Alzheimers Dement.* **14**, 535–562. https://doi.org/10.1016/j.jalz.2018.02.018 (2018).
38. Huang, H. C. et al. Diagnostic accuracy of the Clinical Dementia Rating Scale for detecting mild cognitive impairment and dementia: a bivariate meta-analysis. *Int. J. Geriatr. Psychiatry* **36**, 239–251. https://doi.org/10.1002/gps.5436 (2021).
39. Li, Y. et al. Item response theory analysis of the Clinical Dementia Rating. *Alzheimers Dement.* **17**, 534–542. https://doi.org/10.1002/alz.12210 (2021).
40. Tsoi, K. K. et al. Cognitive tests to detect dementia: a systematic review and meta-analysis. *JAMA Intern. Med.* **175**, 1450–1458. https://doi.org/10.1001/jamainternmed.2015.2152 (2015).
41. Mitchell, A. J. A meta-analysis of the accuracy of the mini-mental state examination in the detection of dementia and mild cognitive impairment. *J. Psychiatr. Res.* **43**, 411–431. https://doi.org/10.1016/j.jpsychires.2008.04.014 (2009).
42. Muntal Encinas, S., Gramunt-Fombuena, N., Badenes Guia, D., Casas Hernanz, L. & Aguilar Barbera, M. Traducción y adaptación española de la batería neuropsicológica Repeatable Battery for the Assessment of Neuropsychological Status (RBANS) forma A en una muestra piloto. *Neurologia* **27**, 531–546. https://doi.org/10.1016/j.nrl.2011.07.006 (2012).
43. Freilich, B. M. & Hyer, L. A. Relation of the Repeatable Battery for Assessment of Neuropsychological Status to measures of daily functioning in dementia. *Psychol. Rep.* **101**, 119–129. https://doi.org/10.2466/pr0.101.1.119-129 (2007).
44. Duff, K. et al. Utility of the RBANS in detecting cognitive impairment associated with Alzheimer's disease: sensitivity, specificity, and positive and negative predictive powers. *Arch. Clin. Neuropsychol.* **23**, 603–612. https://doi.org/10.1016/j.acn.2008.06.004 (2008).
45. Yin, L. et al. The power of the Functional Activities Questionnaire for screening dementia in rural-dwelling older adults at high-risk of cognitive impairment. *Psychogeriatrics* **20**, 427–436. https://doi.org/10.1111/psyg.12524 (2020).
46. Potashman, M. et al. Psychometric properties of the Alzheimer's Disease Cooperative Study - Activities of Daily Living for Mild Cognitive Impairment (ADCS-MCI-ADL) scale: a post hoc analysis of the ADCS ADC-008 trial. *BMC Geriatr.* **23**, 124. https://doi.org/10.1186/s12877-022-03527-0 (2023).
47. Peña-Bautista, C. et al. Clinical utility of plasma lipid peroxidation biomarkers in Alzheimer's disease differential diagnosis. *Antioxidants (Basel)* **9**, 649. https://doi.org/10.3390/antiox9080649 (2020).
48. de la Torre, A. et al. Total syntheses and in vivo quantitation of novel neurofuran and dihomo-isofuran derived from docosahexaenoic acid and adrenic acid. *Chemistry* **21**, 2442–2446. https://doi.org/10.1002/chem.201405497 (2015).
49. Sarria-Estrada, S. et al. Reproducibility of qualitative assessments of temporal lobe atrophy in MRI studies. *Radiologia* **57**, 225–228. https://doi.org/10.1016/j.rx.2014.04.002 (2015).
50. Koedam, E. L. et al. Visual assessment of posterior atrophy development of a MRI rating scale. *Eur. Radiol.* **21**, 2618–2625. https://doi.org/10.1007/s00330-011-2205-4 (2011).
51. Fazekas, F., Chawluk, J. B., Alavi, A., Hurtig, H. I. & Zimmerman, R. A. MR signal abnormalities at 1.5 T in Alzheimer's dementia and normal aging. *AJR Am. J. Roentgenol.* **149**, 351–356. https://doi.org/10.2214/ajr.149.2.351 (1987).
52. R Core Team. *R: A Language and Environment for Statistical Computing* (R Foundation for Statistical Computing, 2026).
53. Friedman, J., Hastie, T. & Tibshirani, R. Regularization paths for generalized linear models via coordinate descent. *J. Stat. Softw.* **33**, 1–22. https://doi.org/10.18633/jss.v033.i01 (2010).
54. Kuhn, M. Building predictive models in R using the caret package. *J. Stat. Softw.* **28**, 1–26. https://doi.org/10.18637/jss.v028.i05 (2008).
55. Thiele, C. & Hirschfeld, G. cutpointr: Improved estimation and validation of optimal cutpoints in R. *J. Stat. Softw.* **98**, 1–27. https://doi.org/10.18637/jss.v098.i11 (2021).
56. Wickham, H. *Ggplot2: Elegant Graphics for Data Analysis* (Springer-Verlag, 2016). https://doi.org/10.1007/978-3-319-24277-4_9.
57. Zhang, X. et al. The emerging role of nitric oxide in the synaptic dysfunction of vascular dementia. *Neural Regen. Res.* **20**, 402–415. https://doi.org/10.4103/NRR.NRR-D-23-01353 (2025).
58. Gao, W. et al. Biomarker genes discovery of Alzheimer's disease by multi-omics-based gene regulatory network construction of microglia. *Brain Sci.* **12**, 1196. https://doi.org/10.3390/brainsci12091196 (2022).
59. Zhang, Y. & Kiryu, H. Identification of oxidative stress-related genes differentially expressed in Alzheimer's disease and construction of a hub gene-based diagnostic model. *Sci. Rep.* **13**, 6817. https://doi.org/10.1038/s41598-023-34021-1 (2023).
60. Cioffi, F., Adam, R. H. I., Bansal, R. & Broersen, K. A review of oxidative stress products and related genes in early Alzheimer's disease. *J. Alzheimers Dis.* **83**, 977–1001. https://doi.org/10.3233/JAD-210497 (2021).
61. Peña-Bautista, C. et al. Lipid Peroxidation Assessment in Preclinical Alzheimer Disease Diagnosis. *Antioxidants* **10**, 1043. https://doi.org/10.3390/antiox10071043 (2021).
62. Peña-Bautista, C. et al. Plasma isoprostanoids assessment as Alzheimer's disease progression biomarkers. *J. Neurochem.* **157**, 6. https://doi.org/10.1111/jnc.15183 (2021).
63. Martino-Adami, P. V. et al. Prognostic value of Alzheimer's disease plasma biomarkers in the oldest-old: a prospective primary care-based study. *Lancet Reg. Health Eur.* **45**, 101030. https://doi.org/10.1016/j.lanepe.2024.101030 (2024).
64. Cullen, N. C. et al. Individualized prognosis of cognitive decline and dementia in mild cognitive impairment based on plasma biomarker combinations. *Nat. Aging* **1**, 114–123. https://doi.org/10.1038/s43587-020-00003-5 (2021).

65. Yim, S. et al. Prognostic value of A/T/N biomarkers: comparing plasma and imaging modalities in Alzheimer disease. *Clin. Nucl. Med.* **50**, 1120–1129. https://doi.org/10.1097/RLU.0000000000006088 (2025).
66. Honey, M. I. J. et al. Individualized prediction of clinical progression to dementia using plasma biomarkers in non-demented elderly. *Alzheimers Res. Ther.* **18**, 4. https://doi.org/10.1186/s13195-025-01925-1 (2025).
67. Coomans, E. M. et al. A head-to-head comparison between plasma pTau181 and tau PET along the Alzheimer's disease continuum. *J. Nucl. Med.* **64**(3), 437–443. https://doi.org/10.2967/jnumed.122.264279 (2023).
68. Pan, F.-F. et al. Plasma P-tau217, GFAP, and NfL as biomarkers for Alzheimer's disease: role in disease stratification, pathological progression, and cognitive decline. *Alzheimers Dement.* **21**(12), e70987. https://doi.org/10.1002/alz.70987 (2025).
69. Santangelo, R. et al. Plasma neurofilament light chain levels and cognitive testing as predictors of fast progression in Alzheimer's disease. *Eur. J. Neurol.* **28**, 2980–2988. https://doi.org/10.1111/ene.14999 (2021).
70. Ren, H. et al. Utilizing multimodal models to forecast Alzheimer's disease progression and clinical subtypes. *Health Inf. Sci. Syst.* **14**, 10. https://doi.org/10.1007/s13755-025-00407-w (2025).
71. Prevot, E., Shand, C. & Oxtoby, N. How reproducible are data-driven subtypes of Alzheimer's disease atrophy?. *J. Alzheimers Dis.* **110**, 426–442. https://doi.org/10.1177/13872877251415019 (2026).
72. Aydın, S. Alzhemimer's disease is characterized by lower segregation in resting-state eyes-closed EEG. *J. Med. Biol. Eng.* **44**, 894–902. https://doi.org/10.1007/s40846-024-00917-0 (2024).

Acknowledgements

CC-P acknowledges a postdoctoral "Miguel Servet" grant CPII21/00006- a FIS project PI22/00594 from Health Institute Carlos III and co-funded by the European Union- and a consolidation project from Ministerio de Ciencia e Innovación (Spain) (ref. CNS2022-135327). The authors acknowledge professor Thierry Durand from the Max Mousseron Institute (Montpellier, France) for some lipid peroxidation compounds synthesis. AM-N and AL acknowledge their grants funded by Instituto de Salud Carlos III through the project FORT23/00021 of the Fortalece program from the Ministerio de Ciencia e Innovación.

Author contributions

A.M.-N., A.L., L.A.-S., S.B-M., M.P., L.G.-V., L.R., M.B. and C.C.-P. obtained the analytical and clinical data. C.C.-P. and M.B. were involved in planning and supervising the work. A.M.-N. and A.L. processed the biological samples. S.B.-M. analyzed the MRI results. A.M.-N., A.L., and A.B. processed the experimental data and drafted the manuscript. All authors reviewed and agreed to the published version of the manuscript.

Funding

This work was supported by the Instituto de Salud Carlos III Project PI22/00594 and co-funded by European Union, the project FORT23/00021 of the Fortalece program from the Ministerio de Ciencia e Innovación, and Grant CNS2022-135327 funded by MICIU/AEI/10.13039/501100011033 and by the "European Union NextGenerationEU/PRTR".

Declarations

Competing interests

The authors declare no competing interests.

Ethical approval

All procedures performed in studies involving human participants were in accordance with the ethical standards of the institutional and/or national research committee and with the 1964 Helsinki Declaration and its later amendments or comparable ethical standards. The study was approved by the Ethics Committee (CEIC) from Health Research Institute La Fe (Valencia, Spain) (2022–282-1 and 2022–990-1).

Patient consent

All participants signed informed consent before their recruitment.

Additional information

Correspondence and requests for materials should be addressed to C.C.-P.

Reprints and permissions information is available at www.nature.com/reprints.

Publisher's note Springer Nature remains neutral with regard to jurisdictional claims in published maps and institutional affiliations.

Open Access This article is licensed under a Creative Commons Attribution-NonCommercial-NoDerivatives 4.0 International License, which permits any non-commercial use, sharing, distribution and reproduction in any medium or format, as long as you give appropriate credit to the original author(s) and the source, provide a link to the Creative Commons licence, and indicate if you modified the licensed material. You do not have permission under this licence to share adapted material derived from this article or parts of it. The images or other third party material in this article are included in the article's Creative Commons licence, unless indicated otherwise in a credit line to the material. If material is not included in the article's Creative Commons licence and your intended use is not permitted by statutory regulation or exceeds the permitted use, you will need to obtain permission directly from the copyright holder. To view a copy of this licence, visit http://creativecommons.org/licenses/by-nc-nd/4.0/.

© The Author(s) 2026